THE JOURNAL OF PHYSICAL CHEMISTRY B

Article

pubs.acs.org/JPCB

Redox Properties of Lysine- and Methionine-Coordinated Hemes Ensure Downhill Electron Transfer in $NrfH_2A_4$ Nitrite Reductase

Smilja Todorovic,* Maria Luísa Rodrigues, Daniela Matos, and Inês A. C. Pereira*

Instituto de Tecnologia Química e Biológica, Universidade Nova de Lisboa, Av. da Republica, 2780-157 Oeiras, Portugal

Supporting Information

ABSTRACT: The multiheme NrfHA nitrite reductase is a menaquinol:nitrite oxidoreductase that catalyzes the 6-electron reduction of nitrite to ammonia in a reaction that involves eight protons. X-ray crystallography of the enzyme from *Desulfovibrio vulgaris* revealed that the biological unit, $NrfH_2A_4$, houses 28 *c*-type heme groups, 22 of them with low spin and 6 with pentacoordinated high spin configuration. The high spin hemes, which are the electron entry and exit points of the complex, carry a highly unusual coordination for *c*-type hemes, lysine and methionine as proximal ligands in NrfA and NrfH, respectively. Employing redox titrations followed by X-band EPR spectroscopy and surface-enhanced resonance Raman spectroelectrochemistry, we provide the first experimental evidence for the midpoint redox potential of the NrfH menaquinol-interacting methionine-coordinated heme (−270 ± 10 mV, z = 0.96), identified by the use of the inhibitor HQNO, a structural analogue of the physiological electron donor. The redox potential of the catalytic lysine-coordinated high spin heme of NrfA is −50 ± 10 mV, z = 0.9. These values determined for the integral $NrfH_2A_4$ complex indicate that a driving force for a downhill electron transfer is ensured in this complex.

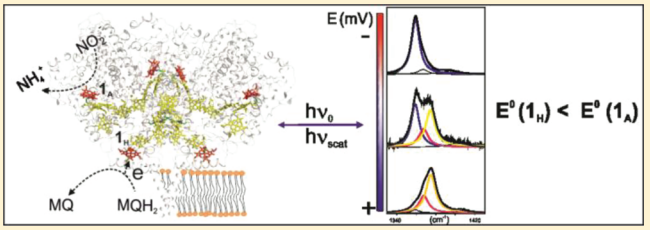

INTRODUCTION

Dissimilatory cytochrome *c* nitrite reductases (ccNiR or NrfA) are pentahemic proteins that catalyze the last step in prokaryotic nitrite ammonification, a key process in the biogeochemical cycling of nitrogen.[1,2] The source of electrons for reduction of nitrite by NrfA is the menaquinone (MQ) pool. There are two alternative biological systems that can carry out this process: (i) In enteric Gammaproteobacteria, such as *E. coli*, the direct electron donor to NrfA is the soluble pentahemic cytochrome NrfB, with which NrfA forms only a transient electron transfer (ET) complex.[3] NrfB, in turn, receives electrons from the membrane-associated NrfCD complex. (ii) In the second, more widespread arrangement, NrfA forms a stable membrane-bound complex with another electron donor NrfH, which receives electrons directly from menaquinol (MQH_2).[1] The latter is present in several classes of bacteria, including Delta- and Epsilonproteobacteria (such as *Wolinella succinogenes* and *Desulfovibrio* spp.), Clostridia, Bacilli, or Bacteroides.[4] NrfH is a membrane-associated tetraheme cytochrome *c* that belongs to a large family of bacterial cytochromes involved in ET from the MQH_2 to periplasmic reductases.[1,4,5] This recently recognized family of quinol dehydrogenases, named NrfH/NapC, includes other proteins such as NapC, the electron donor to the NapAB nitrate reductase,[5] NirT, the electron donor to the cd_1 nitrite reductase,[6] DorC, the electron donor to the DorA dimethylsulfoxide reductase,[7] TorC, the electron donor to the trimethylamine-*N*-oxide reductase,[8] CymA, involved in ET to several reductases,[9] and also the cytochrome c_{m552} that acts in reverse manner, reducing the quinone pool with electrons supplied by hydroxylamine oxidation.[10]

The only structural information available for the NrfH/NapC family of cytochromes is provided by the crystal structure of the NrfH in complex with NrfA from *Desulfovibrio vulgaris*.[11] This stable $NrfH_2A_4$ complex is composed of two $NrfHA_2$ units, where each catalytic NrfA dimer is interacting with one membrane-associated NrfH protein (Figure 1). It comprises an impressive total of 28 heme groups in the biological unit. The two NrfH subunits receive electrons from the membrane quinone pool and transfer them to NrfA, where the reduction of nitrite takes place. The active site in the NrfA subunit (one per NrfA monomer) is a penta-coordinated high spin (5cHS) heme with a highly unusual lysine residue as the axial ligand (heme 1_A) at the proximal side, in a CXXCK heme *c*-binding motif rather than the usual CXXCH. NrfA houses four other bis-His coordinated low spin (LS) hemes *c*, which participate in ET from NrfH to the catalytic site. They are all positioned within distances that allow direct electron tunnelling, as shown by several available X-ray structures.[2,11−15] Each membrane anchoring NrfH subunit houses three LS and one HS heme. Two of the NrfH hemes also show very unusual coordination, as revealed by the crystal structure.[11] The NrfH heme 1 (heme 1_H), which is positioned closest to the membrane, is a 5cHS heme despite the presence of an aspartate residue (Asp89 in *D. vulgaris* NrfH numbering) at the position of the distal axial

Received: February 10, 2012
Revised: March 23, 2012
Published: April 21, 2012

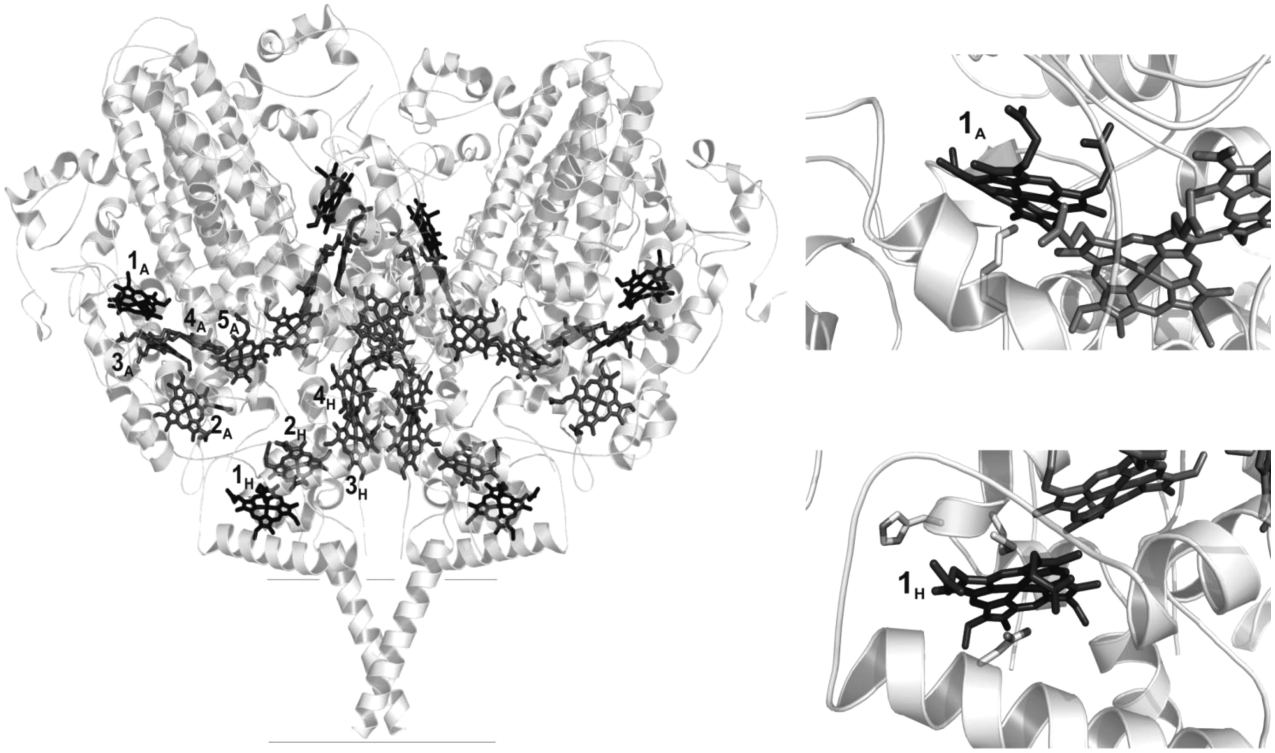

Figure 1. Structural model of $NrfH_2A_4$ (PDB code 2J7A)[11] with designated heme groups 1_A–5_A in NrfA and 1_H–4_H in NrfH (left panel) and close-up of high spin hemes 1_A (top right panel) and 1_H (bottom right panel).

ligand. This heme is coordinated by a conserved methionine positioned two residues after the usual proximal histidine ligand (CXXCHXM). The NrfH heme 4 is a LS heme carrying remarkable His-Lys coordination. The distal lysine residue belongs to the NrfA protein, contributing to the stability of the complex. The $NrfH_2A_4$ complex therefore includes three novel types of heme coordination (HS-Lys, HS-Met, and LS-His/Lys) that require further characterization. However, in a background of 20 bisHis coordinated LS hemes, this represents a considerable spectroscopic challenge.

Mechanistic features of cytochrome c nitrite reductases have been thoroughly studied by experimental and theoretical approaches.[2,4,11−23,26−32] A recent finding that they possess a promising role in the development of biosensors for nitrite detection[33,34] further justifies more detailed investigations. Electrochemical and spectroscopic methods have been employed for determination of the midpoint potentials (E^0) of the cofactors, as a prerequisite for understanding the functioning of these enzymes. The published data provide a consensus that the E^0 values of the heme groups span over a wide range, but reveal some discrepancy between redox potentials of several enzymes from different organisms.[15,27−31] This is not surprising given the high number of hemes, which makes it very difficult to unambiguously separate contributions from different heme groups. Previous studies also revealed some insights into the overall redox behavior of $NrfH_2A_4$;[21] however, a tentative assignment of redox potentials to individual hemes relied on subunits dissociated by a denaturing agent,[28] making it difficult to ascertain their (physiological) relevance. In addition, the analysis of the X-band EPR spectra is complicated by strong spin−spin interactions, while the electrochemical methods, on the other hand, do not provide structural information about the involved species. Surface-enhanced resonance Raman (SERR) spectroelectrochemistry represents a powerful alternative. We have shown previously that the contributions from LS and the HS hemes in the ferric $NrfH_2A_4$ from *D. vulgaris* can be separated on the basis of the respective RR vibrational signatures.[20] In this work, we have employed SERR spectroelectrochemistry[24,25,35−37] to study redox properties of $NrfH_2A_4$. The use of the common reductant, sodium dithionite, which generates anions that can bind to the HS hemes, and affect redox potentials, was therefore avoided.[15] Moreover, the HS hemes are directly observable and do not require labeling by CO, which readily displaces His ligand and binds to LS hemes in some proteins.[27] We report direct evidence for the redox potentials of the hemes 1_H and 1_A that represent the electron entry and electron exit sites in the $NrfH_2A_4$ complex. The data are supported by X-band EPR redox titrations, which provided the spectroscopic signature of the uncoupled HS hemes. These results are further discussed in terms of the redox behavior of other quinol dehydrogenases.

EXPERIMENTAL SECTION

Protein Purification. The $NrfH_2A_4$ protein was purified as a 300 kDa complex, suggesting $\alpha_4\beta_2$ arrangement, from *Desulfovibrio vulgaris* Hildenborough membranes as previously described,[11] using the *n*-dodecyl-β-D-maltoside (DM) detergent for protein solubilization.

EPR Spectroscopy. Potentiometric titrations were performed using ~20 μM $NrfH_2A_4$ (in 50 mM Tris-HCl pH 7.6, 0.025% DM) in the presence/absence of 0.5 mM HQNO (2-*n*-heptyl-4-hydroxyquinoline *N*-oxide). Titrations were performed inside an anaerobic chamber (95% Ar, 5% H_2) at 20 °C, using 100 mM zinc reduced methyl viologen as reductant and a mixture of the following redox mediators: 1,2-naphthoquinone, phenazine methosulfate, phenazine ethosulfate, methylene blue,

dx.doi.org/10.1021/jp301356m | J. Phys. Chem. B 2012, 116, 5637−5643

indigo tetrasulfonate, indigo trisulfonate, indigo disulfonate, 2-hydroxy-1,4-naphthoquinone, safranine, neutral red, benzyl viologen, methyl viologen, and antraquinone-2-sulfonate, at 85 μM final concentration each. The Ag/AgCl and Pt electrodes were calibrated with quinhydrone. Samples were transferred to EPR tubes under anaerobic conditions and immediately frozen in liquid nitrogen.

EPR spectra were recorded on a Bruker EM spectrometer, equipped with an ESR-900 liquid helium cryostat from Oxford Instruments, at 7 K, using microwave frequency of 9.39 GHz, microwave power of 2.4 mW, modulation frequency of 100 kHz, and modulation amplitude of 1 mT.

Surface-Enhanced Resonance Raman (SERR) Spectroscopy. Ag working electrodes were polished and electrochemically roughened following published procedures, and then placed into a homemade electrochemical cell equipped with an Ag/AgCl reference electrode and a Pt counter electrode.[38] Protein immobilization was achieved by spontaneous adsorption onto a detergent (DM)-coated Ag electrode, from the buffer solution (50 mM Tris pH 7.6, 0.1% DM) containing 0.03 μM protein.[24] The cell potential was controlled by a PAR 263-A potentiostat. SERR spectra were collected in backscattering geometry using a confocal microscope coupled to a double monochromator (Jobin Yvon U1000) equipped with 1200 L/mm grating and liquid-nitrogen-cooled back-illuminated CCD detector. All measurements were performed with 413 nm excitation. The spectra were obtained with a long working distance objective (20×, N.A. 0.35), 2 mW laser power, and 30 s accumulation time. Typically, 4 spectra were collected and averaged. RR spectra were recorded from 30 μM protein solution in the resting or $NaBH_4$ reduced state, with 40 s accumulation time and 1 mW laser power. Spectroelectrochemical SERR titrations were performed in the −400 to +350 mV range, with 20−50 mV steps. At each potential, the system was allowed to equilibrate for 2 min, as was found to be sufficient for reaching the equilibrium state. The measurements in the presence of inhibitor were performed upon addition of 20−50× excess of HQNO (50 mM EtOH solution) to the spectroelectrochemical cell containing the solubilized protein, prior to immobilization.

Spectral Analysis. The contributions of the HS and LS ferric and total ferrous populations were determined in each spectrum from deconvolution of the ν_4 band into $\nu_{4,oxHS}$, $\nu_{4,oxLS}$, and $\nu_{4,red}$ using the same line width and frequency ($\nu_{4,oxHS}$ 1366 cm^{-1}, $\Delta\nu_{4,oxHS}$ 12.8 cm^{-1}; $\nu_{4,oxLS}$ 1374 cm^{-1}, $\Delta\nu_{4,oxLS}$ 13.8 cm^{-1}; $\nu_{4,red}$ 1357 cm^{-1}, $\Delta\nu_{4,red}$ 9.9 cm^{-1}). The relative intensities of the respective ν_4 species were determined from the best fit of the component spectra to the experimental one, for each potential, and were plotted as a function of applied potential.[24,25]

Redox potentials were determined from the fit of the relative intensities of ν_4 (I_{ox}^{rel}) to the Nernst equation (eq 1), for $n = 2$ transitions, treating the reduction potential and number of transferred electrons (z) as adjustable parameters:

$$I_{ox}^{rel} = \sum_{i=1}^{n} \frac{1}{1 + \exp\left[-\frac{zF}{RT}(E - E_i^0)\right]} \quad (1)$$

All potentials cited in this work refer to the NHE.

RESULTS

EPR Spectroscopy. The X-band EPR spectra of $NrfH_2A_4$ in the resting state are dominated by the resonances that originate from highly spin-coupled systems, Figure 2, trace a. These include the strong signals at g_{max}= 3.6 and 3.3, which have been

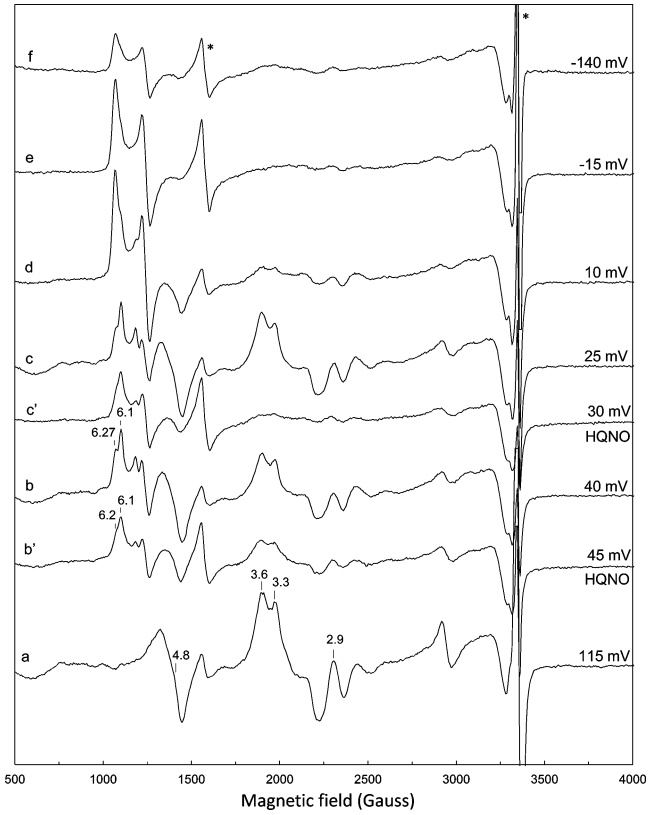

Figure 2. Redox titration of $NrfH_2A_4$ (traces a−f) and $NrfH_2A_4$:HQNO complex (traces b′, c′), followed by X band EPR spectroscopy; EPR spectra are measured at 7 K, using microwave frequency of 9.39 GHz, microwave power of 2 mW, modulation frequency of 100 kHz, and modulation amplitude of 1 mT. The resonances at $g \approx 2$ and at $g = 4.3$, marked by asterisk, originate from the mediator cocktail and zinc-reduced methyl viologen, respectively.[21]

assigned to a coupled pair of LS and HS hemes;[15,22,39] the signal at $g = 2.9$, 2.27, and 1.5; and the prominent resonance at $g = 4.8$, which is characteristic of the presence of NrfH bound to NrfA,[22,40] as this signal is not observed in the spectrum of isolated NrfA.[15] Thus, the HS hemes (i.e. hemes 1_H and hemes 1_A) are not directly observable in the spectra of the oxidized $NrfH_2A_4$ complex due to coupling with neighboring LS hemes (i.e. heme 2_H and heme 3_A in the NrfH and NrfA, respectively), Figure 1. However, the spectral contributions from the HS hemes can be revealed by stepwise reduction of $NrfH_2A_4$,[21] indicating that the coupling LS hemes have more positive and well-separated redox potentials. The presence of two rhombic HS signals, (i) at $g_{max} = 6.10$, $g_{med} = 5.63$, and $g_{min} \approx 2$, and (ii) at $g_{max} = 6.27$, $g_{med} = 5.43$, and $g_{min} \approx 2$, becomes evident at potentials ≤40 mV (Figure 2, trace b). Along the titration, the former species becomes reduced first and therefore EPR silent (Figure 2, trace e). The values of E/D, estimated from g_{max} and g_{med} (and $S = \pm 1/2$ transitions), are approximately 0.004 for $g_{max} = 6.1$ and 0.013 for the $g_{max} = 6.27$ signal, revealing the very weak character of proximal ligands of both HS populations.

In the next step, the redox titrations were performed in the presence of HQNO, an analogue of MQH_2, which binds in close proximity to heme 1_H.[23] We observed noticeable alterations in the HS region of the EPR spectra. In particular,

dx.doi.org/10.1021/jp301356m | J. Phys. Chem. B 2012, 116, 5637−5643

the HS population characterized by g_{max} = 6.27 in the absence of HQNO undergoes a shift to 6.20 in its presence (Figure 2, trace c), suggesting the assignment of these resonances to heme 1_H. Although small, these alterations reveal a further decrease of rhombicity of the heme 1_H symmetry.

SERR Spectroelectrochemistry. We employed SERR spectroscopy using Soret band excitation to probe the redox properties of $NrfH_2A_4$ immobilized on biocompatible metal electrodes. This strategy that relies on the analysis of the redox-sensitive vibrational fingerprints of the heme groups was previously successfully applied in the studies of other multiple-heme containing proteins.[24,25] A key issue in this approach is preservation of the native structure of the protein upon immobilization. To that end, a number of methodologies for adsorption of soluble and membrane proteins has been developed, mainly based on functionalization of the metal surface by self-assembled monolayers of alkane thiols.[37] For immobilization of $NrfH_2A_4$, and membrane complexes in general, one can take advantage of the presence of detergent molecules that ensure protein solubilization. The immobilization then takes place via interactions of the detergent molecules with the layer of specifically adsorbed anions that the metal surface carries above the potential of zero-charge, providing a biocompatible interface for subsequent protein adsorption.[24]

A careful comparison of the RR and SERR spectra, Figure 3, reveals that no major alterations on the level of heme groups

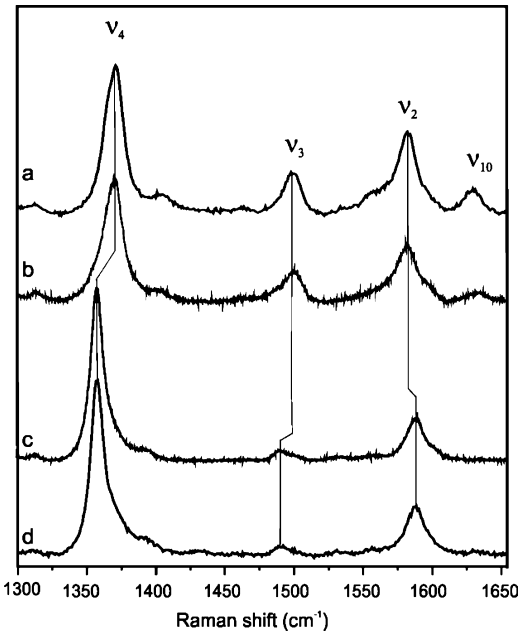

Figure 3. RR spectra of ferric (a) and ferrous (d) $NrfH_2A_4$ in solution and SERR spectra of ferric (b) and ferrous (c) $NrfH_2A_4$ immobilized on DM-coated electrode. All spectra were recorded at room temperature, with 413 nm excitation, and laser power and accumulation time of 2 mW and 30 s (SERR) or 1 mW and 40 s (RR).

occur upon immobilization of $NrfH_2A_4$. The positions of the high frequency bands ν_4, ν_3, ν_2, and ν_{10}, which are sensitive reporters of the redox, coordination, and spin state of the heme iron, are well reproduced in the SERR spectra, and no additional bands or band broadening appear. Small variations in the relative band intensities can be attributed to the orientation dependence of the SERR effect.[24] At the most negative potential (−400 mV), the protein appears fully reduced, as judged by the frequencies of ν_4, ν_3, and ν_2, found at 1357, 1490, and 1588 cm^{-1}, respectively (Figure 3, trace c). At potential poised at +350 mV, all heme groups are oxidized, as indicated by the ν_4, ν_3, ν_2, and ν_{10} modes that are found at 1374, 1501, 1583, and 1625 cm^{-1}, respectively (Figure 3, trace b).

Component analysis of the ν_4/ν_3 region of the spectra (vide infra) further reveals that the same band frequencies and linewidths defined previously in the RR spectra of ferric and ferrous $NrfH_2A_4$ in solution have to be used for the best fit of the component spectra to the experimental SERR data.[20]

Moreover, the relative $\nu_{4,oxHS}/\nu_{4,oxLS}$ intensity ratio in the SERR spectra of the ferric protein corresponds to the one determined earlier in RR spectra,[20] indicating that no additional HS species were formed upon protein adsorption. Therefore, we concluded that the protein retains its native structure upon immobilization. The SERR spectra of adsorbed $NrfH_2A_4$ responded sensitively to the applied potential. The potential-dependent SERR spectra could be quantitatively reproduced independently of the sequence of applied electrode potentials, indicating that the redox processes are fully reversible. A small population of immobilized protein (<6%), however, was insensitive to applied potential, as shown by the component analysis, Figure 4. We attribute this fraction to protein immobilized in an unfavorable orientation for efficient heterogeneous ET. The intensity of the ν_4 band was corrected for this residual fraction in the further data analysis (vide infra).

A series of potential-dependent SERR spectra were submitted to component analysis to determine relative contributions of the ferrous versus ferric species at each potential. The analysis was limited to the most prominent band ν_4,[25] which is also the most sensitive indicator of the redox state, and, in addition, shows well-separated features of ferric HS and LS hemes in $NrfH_2A_4$ (Figure 4, bottom trace).[20] The (SE)RR spectra of the ferrous $NrfH_2A_4$, on the other hand, allow only for the determination of the total contribution of the reduced species (Figure 4, top and middle traces).

At each potential, the ν_4 envelope, containing ferric ($\nu_{4,oxHS}$ 1366 cm^{-1}, $\Delta\nu_{4,oxHS}$ 12.8 cm^{-1} and $\nu_{4,oxLS}$ 1374 cm^{-1}, $\Delta\nu_{4,oxLS}$ 13.8 cm^{-1}) and/or ferrous ($\nu_{4,red}$ 1357 cm^{-1}, $\Delta\nu_{4,red}$ 9.9 cm^{-1}) contributions, was fitted with Lorentzian bands with fixed positions and widths to determine the total contributions of the respective species. The potential dependence of the normalized ν_4 intensity of the ferric HS population obtained with this treatment is shown in Figure 5a, where each point represents the average of at least 3−6 independent determinations. The best fit of eq 1 to the experimental data, for n = 2 transitions, treating the reduction potential and number of transferred electrons (z) as adjustable parameters, revealed two well -separated transitions for HS population (Figure 5a): at −270 mV, z = 0.96, and at −50 mV, z = 0.88. Because of the presence of numerous LS hemes with coordination patterns that are indistinguishable by (SE)RR, no attempt to analyze their redox behavior in detail was made. However, data reveal that the redox potentials of the LS hemes can be approximately grouped around −170 and −5 mV (Supporting Information, Figure SI 1). The two transitions are broad, further indicating unresolved redox transitions within the two intervals.

In the next step, spectroelectrochemical titrations were carried out in the presence of excess of HQNO. The ν_4 region of the potential-dependent SERR spectra was deconvoluted using the band parameters determined before (vide supra). The fit of the relative intensity of the $\nu_{4,oxHS}$ band as a function of potential to eq 1 shows two transitions with E^0 = −320 ± 10

dx.doi.org/10.1021/jp301356m | J. Phys. Chem. B 2012, 116, 5637−5643

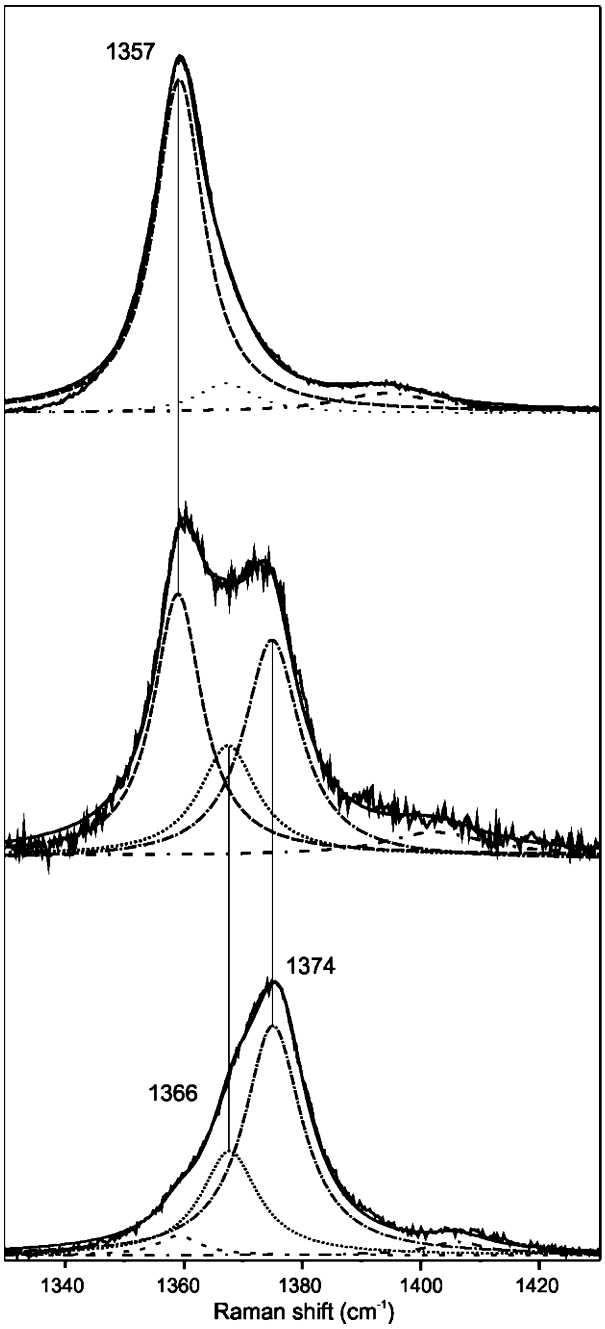

Figure 4. The potential-dependent SERR spectra of immobilized $NrfH_2A_4$. The ν_4 region of experimental and component SERR spectra of $NrfH_2A_4$ in ferrous (top trace), intermediate (middle trace), and ferric (bottom trace) redox states, measured at electrode potential poised at −300, −50, and +250 mV, respectively. Component spectra represent total ferrous (dashed line), HS ferric (dotted line), and LS ferric (dash−dotted line) population. The residual, nonelectroactive populations in the top (dotted line, large spacing) and bottom traces (dashed line, large spacing) are designated, as well as the contributions from the ν_{20} (dash−dash−dotted line, large spacing).

mV, z = 0.95, and E^0 = −70 ± 10 mV, z = 0.88, Figure 5b. The data reveal an approximately 50 mV downshift of the redox potential associated with one HS population, while the other transition remains constant, within the error of determination. Therefore, we assign the redox potentials of −270 and −50 mV, obtained by spectroelectrochemical titration of $NrfH_2A_4$ in the absence of HQNO, to heme 1_H and to heme 1_A, respectively.

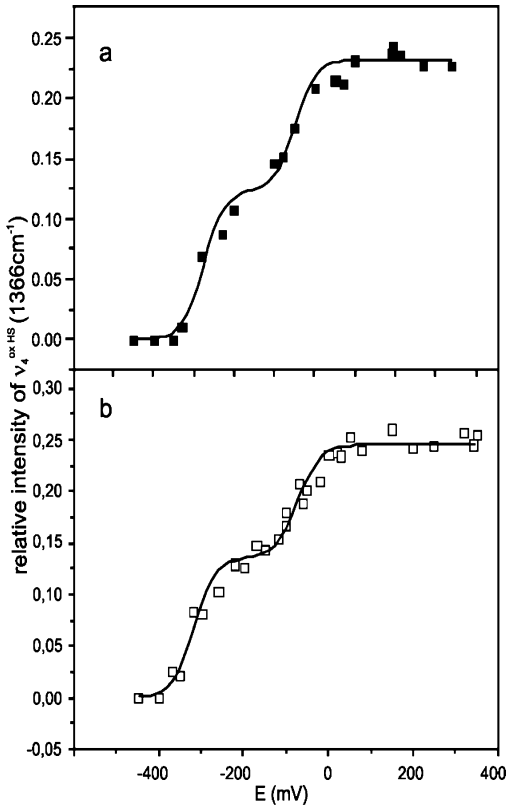

Figure 5. SERR spectroelectrochemical titration of $NrfH_2A_4$ immobilized on DM coated electrode, (a) in the absence and (b) in the presence of HQNO. Data points correspond to relative ν_4 band intensity of ferric HS (1366 cm^{-1}) population. The curves represents the best fit of experimental data to eq 1, for n = 2 and E^0 and z treated as adjustable variables, indicating two transitions with: (a) E^0 = −270 ± 10 mV, z = 0.96, and E^0 = −50 ± 10 mV, z = 0.88; and (b) E^0 = −320 ± 10 mV, z = 0.95, and E^0 = −70 ± 10 mV, z = 0.88.

The EPR data support this finding, as they point to a lower redox potential of the Met-coordinated heme 1_H.

There is a reasonably good agreement between the redox potential of heme 1_A (−50 mV), determined here employing the intact $NrfH_2A_4$ complex and direct heterogeneous ET, with that reported for the corresponding heme in *D. desulfuricans* (−80 mV)[32] and *E. coli* NrfA homodimer (−107 mV).[15] For the redox potential of 5cHS Met-coordinated heme 1_H, however, there are no data available in the literature. The value that we observe here (E^0 = −270 mV) appears lower than expected, because the MQH_2:nitrite oxidoreductase activity of $NrfH_2A_4$ relies on ET from MQH_2 to heme 1_H, suggesting a redox potential for this heme close or slightly higher than the E^0 (MQ/MQH_2) of −70 mV. Interestingly, other members of the NrfH/NapC family, such as NapC, DorC, and TorC, also possess redox potentials more negative than E^0 (MQ/MQH_2).[5,7,8] This difference may indicate a presence of a conformational switch at onset of the ET pathway in these proteins. Clearly, understanding of the parameters that control the quinol oxidation in $NrfH_2A_4$ and other quinol dehydrogenases requires further studies.

DISCUSSION

Herein, we present a spectroscopic and thermodynamic characterization of the HS hemes in $NrfH_2A_4$ cytochrome *c* nitrite reductase complex. The pentahemic catalytic NrfA

dx.doi.org/10.1021/jp301356m | J. Phys. Chem. B 2012, 116, 5637−5643

protein has been thoroughly studied, due to the fact that it can be purified in a stable form from some organisms.[15,29−31] The situation is more intricate in the case of NrfH because, to date, it has only been isolated as a membrane complex with NrfA.[21,22,28,32] In *D. vulgaris*, this complex comprises 28 heme groups, representing a challenge for any experimental approach.

The X-ray structure of the *D. vulgaris* $NrfH_2A_4$ complex revealed a highly unusual coordination of the heme 1_H, with a methionine residue as proximal heme ligand and an aspartate residue occupying the distal heme position, but not coordinating the heme iron.[11,23] Sequence alignments suggest that the NrfH fold, diheme stacking motif of the four hemes *c* (1_H−2_H and 3_H−4_H), and quinol binding site are likely to be shared by other members of the bacterial membrane-anchored tetra- or penta-hemic cytochromes *c* from the NrfH/NapC protein family.[4] Indeed, recent homology models of CymA from *Shewanella* sp. ANA-3[41] and cyt c_{m552} from *Nitrosomonas europaea*,[10] based on the *D. vulgaris* NrfH structure, predict that the heme 1_H is penta-coordinated, and that the main features of the quinol/quinone binding site are preserved in these proteins. However, spectroscopic evidence for the presence of HS heme was observed only in cytochrome c_{m552} and assigned to heme 1, predicted to carry a Met axial ligand.[10] The spectroscopic characterization of other members of NrfH/NapC family, including NapC,[5] DorC,[7] CymA,[42] and TorC,[8] failed to reveal the presence of HS hemes, indicating that the coordination of heme 1 may be different from that of heme 1_H, or that the HS heme is obscured by spin−spin coupling. Our previous EPR data suggested the presence of two HS hemes in the $NrfH_2A_4$ complex,[21] but did not provide sufficient evidence for assignment of the resonances. Here, we report two distinct HS species in the EPR spectra, one with g_{max} = 6.10, g_{med} = 5.63 that we assign to the Lys-coordinated heme 1_A and the other with g_{max} = 6.27, g_{med} = 5.43 that we assign to the Met-coordinated heme 1_H, based on the alterations of the latter resonances in the presence of HQNO that selectively binds in the vicinity of the heme 1_H (vide infra). Moreover, we observe that both atypical axial ligands reveal exceptionally weak character, as indicated by the E/D values. In the next step, we characterized the thermodynamic properties of these unusual hemes. The spectroelectrochemical approach that we have employed is largely free of uncertainties associated with other techniques, at least for the HS hemes that can be directly monitored by SERR spectroscopy. In addition, due to the potential drop at the electrode/DM coating/$NrfH_2A_4$ interface, the immobilized protein senses electric fields comparable with the membrane potential that can modulate the ET processes in membrane associated proteins.[24,25,35−37] Under these conditions, we show that the redox transition associated with one HS heme population undergoes a downshift of 50 mV in the presence of HQNO, allowing its assignment to the heme 1_H. The binding of HQNO or analogous compounds typically affects both spectroscopic properties and reduction potentials of heme groups in proteins that possess quinol binding sites, as observed for example in nitrate reductases (NarGHI),[43−45] succinate:quinone oxidoreductases,[46] formate dehydrogenase,[47] and cytochrome b_6f.[48] The direction and magnitude of the change of redox potential vary among different proteins, and it can be as drastic as −225 mV in the case of the heme c_n of cytochrome b_6f.[49] Being structurally similar to a semiquinone intermediate, HQNO occupies the MQH_2 binding site and therefore acts as a competitive inhibitor of the NrfH:MQH_2 oxidase activity.[23] It binds in the distal cavity of NrfH as demonstrated by X-ray crystallography,[23] causing minor structural rearrangements. Because the presence of HQNO does not appear to alter the RR spectra of $NrfH_2A_4$ in solution or the SERR spectra of the immobilized protein, we can discard major structural changes in the pocket of heme 1_H as the origin of the potential shift. Rather, subtle structural changes together with alterations of the electrostatics of the surrounding environment may be the origin of this shift, as observed in other heme proteins.[35] The redox potential of a heme group is fine-tuned by an interplay of the influences imposed by axial coordination and hydrophobicity of the surrounding medium. Increased hydrophobicity of the heme pocket can produce an upshift of the redox potential by 200−300 mV, while deprotonation of the proximal imidazole, for instance, is capable of lowering the redox potential by 700 mV.[50,51] The downshift of the $E^0(1_H)$ that we observe here indicates that the ferric state, which has formal +1 positive charge, is stabilized. This suggests that water molecules may have an increased access to the heme cavity in the presence of HQNO. Crystallographic and molecular dynamics data indeed reveal a largely polar MQH_2 binding cavity in NrfH, with a wide opening to the solvent that facilitates diffusion of the six MQH_2 molecules that are required to complete the catalytic reaction at the associated NrfA dimer.[23] The lowering of the redox potential of the heme 1_H in the presence of MQH_2, by analogy to the effect observed with HQNO, may also act to facilitate the biological ET by increasing the overall driving force. Thermodynamic considerations further imply that MQH_2 binds more tightly to the ferric NrfH,[49] which further helps to drive the physiological ET from the quinol to the NrfH hemes, from there to the NrfA hemes, and finally to nitrite.

The present work provides the first solid experimental evidence for the redox potential of heme 1_H in the integral $NrfH_2A_4$, therefore contributing to disentangling of the complex ET pathway in this large protein. We show that the electron entry point (heme 1_H) has a substantially lower redox potential than the catalytic heme where the reduction of nitrite occurs (heme 1_A), which ensures downhill biological electron flow in the integral $NrfH_2A_4$complex from *D. vulgaris*.

■ ASSOCIATED CONTENT

Ⓢ Supporting Information

Figure SI 1: SERR titration of $NrfH_2A_4$ showing the relative ν_4 band intensity of the ferric low spin (1374 cm^{-1}) species, as a function of potential. This material is available free of charge via the Internet at http://pubs.acs.org.

■ AUTHOR INFORMATION

Corresponding Author

*E-mail smilja@itqb.unl.pt (S.T.); ipereira@itqb.unl.pt (I.A.C.P.).

Notes

The authors declare no competing financial interest.

■ ACKNOWLEDGMENTS

Financial support from FCT grants PTDC/BIA-PRO/68486/2006 to I.A.C.P. and PTDC/BIA-PRO/100791/2008 to S.T. and FCT/MCTES fellowship SFRH/BPD/24372/2005 to M.L.R. is gratefully acknowledged.

■ ABBREVIATIONS

SERR, surface enhanced resonance Raman; HQNO, 2-*n*-heptyl-4-hydroxyquinoline *N*-oxide; ET, electron transfer; HS, high spin; LS, low spin; DM, *n*-dodecyl-*β*-D-maltoside; MQ, menaquinone; MQH_2, menaquinol

■ REFERENCES

(1) Simon, J. *FEMS Microbiol. Rev.* **2002**, *26*, 285−309.
(2) Einsle, O. *Methods Enzymol.* **2011**, *496*, 399−422.
(3) Clarke, T.; Cole, J. A.; Richardson, D. J.; Hemmings, A. M. *Biochem. J.* **2007**, *406*, 19−30.
(4) Rodrigues, M. L.; Pereira, I. A. C.; Archer, M. In *Handbook of Metalloproteins*; Messerschmidt, A., Ed.; John Wiley & Sons Ltd.: Chichester, 2011; pp 89−102.
(5) Roldan, M.; Sears, H. J.; Cheesman, M.; Ferguson, S. J.; Thomson, A. J.; Berks, B. C.; Richardson, D. *J. Biol. Chem.* **1998**, *273*, 28785−28790.
(6) Jungst, A.; Wakabayashi, S.; Matsubara, H.; Zumft, W. G. *FEBS Lett.* **1991**, *279*, 205−209.
(7) Shaw, A. L.; Hochkoeppler, A.; Bonora, P.; Zannoni, D.; Hanson, G. R.; McEwan, A. G. *J. Biol. Chem.* **1999**, *274*, 9911−9914.
(8) Gon, S.; Giudici-Orticoni, M. T.; Mejean, V.; Iobbi-Nivol, C. *J. Biol. Chem.* **2001**, *276*, 11545−11551.
(9) Myers, J. M.; Myers, C. R. *J. Bacteriol.* **2000**, *182*, 67−75.
(10) Kim, H. J.; Zatsman, A.; Upadhyay, A. K.; Whittaker, M.; Bergmann, D.; Hendrich, M. P.; Hooper, A. B. *Biochemistry* **2008**, *47*, 6539−6551.
(11) Rodrigues, M. L.; Oliveira, T. F.; Pereira, I. A. C.; Archer, M. *EMBO J.* **2006**, *25*, 5951−5960.
(12) Einsle, O.; Messerschmidt, A.; Stach, P.; Bourenkov, G. P.; Bartunik, H. D.; Huber, R.; Kronek, P. M. H. *Nature* **1999**, *400*, 476−480.
(13) Einsle, O.; Stach, P.; Messerschmidt, A.; Simon, J.; Kroger, A.; Huber, R.; Kroneck, P. M. H. *J. Biol. Chem.* **2000**, *275*, 39608−39616.
(14) Cunha, C. A.; Macieira, S.; Dias, J. M.; Almeida, G.; Goncalves, L. L.; Costa, C.; Lampreia, J.; Huber, R.; Moura, J. J. G.; Moura, I.; Romao, M. J. *J. Biol. Chem.* **2003**, *278*, 17455−17465.
(15) Bamford, V. A.; Angove, H. C.; Seward, H. E.; Thompson, A. J.; Cole, J. A.; Butt, J. N.; Hemmings, A. M.; Richardson, D. J. *Biochemistry* **2002**, *41*, 2921−2931.
(16) Einsle, O.; Messerschmidt, A.; Huber, R.; Kroneck, P. M. H.; Neese, F. *J. Am. Chem. Soc.* **2002**, *124*, 11737.
(17) Einsle, O. In *Handbook of Metalloproteins*; Messerschmidt, A., Huber, R., Poulos, T., Wieghardt, K., Eds.; Wiley and Sons: New York, 2001.
(18) Lukat, P.; Rudolf, M.; Stach, P.; Messerschmidt, A.; Kroneck, P. M. H.; Simon, J.; Einsle, O. *Biochemistry* **2008**, *47*, 2080−2086.
(19) Simon, J.; Gross, R.; Einsle, O.; Kroneck, P. M. H.; Kroger, A.; Klimmek, O. *Mol. Microbiol.* **2000**, *35*, 686−696.
(20) Martins, G.; Rodrigues, M. L.; Cunha, F. M.; Matos, D.; Hildebrandt, P.; Murgida, D.; Pereira, I. A. C.; Todorovic, S. *J. Phys. Chem. B* **2010**, *114*, 5563−5566.
(21) Pereira, I. A. C.; LeGall, J.; Xavier, A. V.; Teixeira, M. *Biochim. Biophys. Acta* **2000**, *1481*, 119−130.
(22) Pereira, I. A. C.; Abreu, I. A.; Xavier, A. V.; LeGall, J.; Teixeira, M. *Biochem. Biophys. Res. Commun.* **1996**, *224*, 611−618.
(23) Rodrigues, M. L.; Scott, K.; Sansom, M.; Pereira, I. A. C.; Archer, M. *J. Mol. Biol.* **2008**, *381*, 341−350.
(24) Todorovic, S.; Pereira, M.; Bandeiras, T.; Teixeira, M.; Hildebrandt, P.; Murgida, D. *J. Am. Chem. Soc.* **2005**, *127*, 13561−13566.
(25) Todorovic, S.; Verissimo, A.; Pereira, M.; Teixeira, M.; Hildebrandt, P.; Zebger, I.; Wisitruangsakul, N.; Murgida, D. *J. Phys. Chem. B* **2008**, *112*, 16952−16959.
(26) Bykov, D.; Neese, F. *J. Biol. Inorg. Chem.* **2011**, *16*, 417−430.
(27) Almeida, G.; Silveira, C.; Guigliarelli, B.; Bertrand, P.; Moura, J. J. G.; Moura, I.; Leger, C. *FEBS Lett.* **2007**, *581*, 284−288.
(28) Almeida, G.; Macieira, S.; Gonsalves, L. L.; Huber, R.; Cunha, C. A.; Romao, M. J.; Costa, C.; Lampreia, J.; Moura, J. J. G.; Moura, I. *Eur. J. Biochem.* **2003**, *270*, 3904−3915.
(29) Clarke, T.; Mills, P.; Poock, S.; Butt, J. N.; Cheesman, M.; Cole, J. A.; Hinton, J.; Hemmings, A. M.; Kemp, G.; Soderberg, C.; Spiro, S.; van Wonderen, J.; Richardson, D. *Methods Enzymol.* **2008**, *437*, 64−77.
(30) Gates, A.; Kemp, G.; Yip To, C.; Mann, J.; Marritt, S.; Mayes, A.; Richardson, D.; Butt, J. N. *Phys. Chem. Chem. Phys.* **2011**, *13*, 7720−7731.
(31) Gwyer, J. D.; Angove, H. C.; Richardson, D.; Butt, J. N. *Biochemistry* **2004**, *63*, 43−47.
(32) Costa, C.; Moura, J. J. G.; Moura, I.; Wang, Y.; Huynh, B. H. *J. Biol. Chem.* **1996**, 23191−23196.
(33) Silveira, C.; Gomes, S.; Araujo, A.; Montenegro, C.; Todorovic, S.; Viana, A.; Silva, R.; Moura, J. J. G.; Almeida, G. *Biosens. Bioelectron.* **2010**, *25*, 2026−2032.
(34) Strehlitz, B.; Gründig, B.; Schumacher, W.; Kroneck, P. M.; Vorlop, K. D.; Kotte, H. *Anal. Chem.* **1996**, *68*, 807−816.
(35) Todorovic, S.; Jung, C.; Hildebrandt, P.; Murgida, D. *J. Biol. Inorg. Chem.* **2006**, *11*, 119−127.
(36) Murgida, D.; Hildebrandt, P. *Acc. Chem. Res.* **2004**, *37*, 654−661.
(37) Murgida, D.; Hildebrandt, P.; Todorovic, S. In *Biomimetics, Learning from Nature*; Mukherjee, A., Ed.; In-Tech: Viena, 2010; pp 21−47.
(38) Murgida, D.; Hildebrandt, P. *J. Phys. Chem. B* **2001**, *105*, 1578−1586.
(39) Blackmore, R. S.; Gadsby, P. M. A.; Greenwood, C.; Thompson, A. J. *FEBS Lett.* **1991**, *264*, 257−262.
(40) Schumacher, W.; Hole, U.; Kroneck, P. M. H. *Biochem. Biophys. Res. Commun.* **1994**, *205*, 911−916.
(41) Zargar, K.; Saltikov, C. W. *Arch. Microbiol.* **2009**, *191*, 797−806.
(42) Field, S. J.; Dobbin, P. S.; Cheesman, M.; Watamough, N. J.; Thomson, A. J.; Richardson, D. *J. Biol. Chem.* **2000**, *275*, 8515−8522.
(43) Jormmaka, M.; Tornroth, S.; Byrne, B.; Iwata, S. *Science* **2002**, *295*, 1863−1868.
(44) Rothery, R. A.; Blasco, F.; Magalon, A.; Asso, M.; Weiner, J. H. *Biochemistry* **1999**, *38*, 12747−12757.
(45) Bertero, M. G.; Rothery, R. A.; Boroumand, N.; Palak, M.; Blasco, F.; Ginet, N.; Weiner, J. H.; Strynadka, N. C. *J. Biol. Chem.* **2005**, *280*, 14836−14843.
(46) Smirnova, I. A.; Hagerhall, C.; Konstantinov, A.; Hederstedt, L. *FEBS Lett.* **1995**, *359*, 23−26.
(47) Kroger, A.; Winkler, E.; Innerhofer, A.; Hackenberg, H.; Schagger, H. *Eur. J. Biochem.* **1979**, *94*, 465−475.
(48) Zatsman, A.; Zhang, H.; Gunderson, W. A.; Cramer, W. A.; Hendrich, M. P. *J. Am. Chem. Soc.* **2006**, *128*, 14246−14247.
(49) Alric, J.; Pierre, Y.; Picot, D.; Lavergne, J.; Rappaport, F. *Proc. Natl. Acad. Sci. U.S.A.* **2005**, *102*, 15860−15865.
(50) Kassner, R. *J. Am. Chem. Soc.* **1973**, *95*, 2674−2677.
(51) Nesset, M.; Shokhirev, N.; Enemark, P.; Jacobson, S.; Walker, F. A. *Inorg. Chem.* **1996**, *35*, 5188−5200.